

Tunable topological order of pseudo spins in semiconductor heterostructures

Clemens Kuhlenkamp,^{1,2,3} Wilhelm Kadow,^{1,2} Ataç Imamoğlu,³ and Michael Knap^{1,2}

¹*Department of Physics, Technical University of Munich, 85748 Garching, Germany*

²*Munich Center for Quantum Science and Technology (MCQST), Schellingstr. 4, D-80799 München, Germany*

³*Institute for Quantum Electronics, ETH Zürich, CH-8093 Zürich, Switzerland*

(Dated: September 14, 2022)

We propose a novel platform to realize highly-tunable, frustrated Hubbard physics with topological order in multi-layer moiré structures. Identifying a layer degree of freedom as a pseudo spin, allows us to retain $SU(2)$ symmetry, while controlling ring exchange processes and concurrently quenching the kinetic energy by large external magnetic fields. This way, a broad class of interacting Hofstadter states and their transitions can be studied. Remarkably, in the limit of strong interactions the system becomes Mott insulating and we find exceptionally stable spin liquid phases which are induced by the magnetic field. As the magnetic flux can be easily tuned in moiré systems, our approach provides a promising route towards the experimental realization and control of topologically ordered phases of matter. We also discuss how layer pseudo-spin can be probed in near-term experiments.

Frustrated electronic systems are expected to exhibit a variety of exotic quantum phases, including fractional quantum Hall states and spin liquids, which host intrinsic topological order and emergent gauge fields [1–3]. While these systems have attracted tremendous theoretical and experimental interest, the decade long quest for the experimental realization of such long-range entangled states has been challenged by their fragility. In particular, when topological order is encoded in the spin degree of freedom, a characterization and manipulation of the excitations becomes intractable. Even in theoretical models, spin liquids often appear only for very specific parameters, which makes finding good candidate materials difficult [3, 4]. Consequently, conclusive evidence for spin liquids in solids is hard to find, which makes it essential to identify tunable solid-state platforms that allow for novel probes of the spin liquid states.

The kinetic energy of electrons can be controllably quenched by large, external magnetic fields in moiré heterostructures of transition metal dichalcogenides (TMDs). While these magnetic fields eventually polarize the electron spin, we can retain an $SU(2)$ symmetry by considering synthetic layer pseudo-spins instead of electronic spins [5–7]. The lowest bands of such systems can be described by effective triangular lattice Hubbard models, which makes them particularly promising settings to study the interplay of geometric frustration and strong interactions [8–12]. Here, we show that the magnetic field serves as an additional tuning knob and induces a particularly rich phase diagram, ranging from Hofstadter physics for small interactions to spin-liquid phases in the Mott insulating regime [13–17]. In particular, the magnetic field can reliably tune ring-exchange processes, which help stabilize exceptionally robust chiral spin liquids (CSL) [12, 17, 18]. Due to the large moiré unit-cells it is possible to insert high enough flux to explore the full spectrum of the Hofstadter butterfly [13, 19]. This enables us to study a large variety of phases, including transitions between topological charge

and spin sectors, which are inaccessible for conventional candidate materials.

Frustrated Hubbard physics in twisted TMD bilayers.— Heterostructures of two dimensional (2D) materials form moiré patterns, either if there is a lattice constant mismatch between the materials, or if some of the layers are twisted against each other. This commonly results in honeycomb and triangular structures, which imprint lattices on the electrons. Motivated by recent work [12], we consider triangular moiré patterns, in which two lattices in different layers coincide spatially. This can be achieved in ‘sandwich’ stacked trilayer systems; or for AB-stacked homobilayers with a twist [12, 20], as shown in Fig. 1 a).

Depending on the depth of the lattice potential [21], the lowest lying moiré band of the TMD heterostructure can then realize an effective triangular Hubbard model, with two electronic degrees of freedom: spin and layer. Here we explore the phase diagram of these models by tuning the external magnetic field B_z . Once the Zeeman effect fully polarizes the electrons, their spin can be discarded and the TMD system is described by an interacting Hofstadter-Hubbard model on the triangular lattice:

$$\begin{aligned} \hat{H} = & -t \sum_{\langle ij \rangle, \sigma \in \{T, B\}} e^{i\phi_{ij}} c_{i, \sigma}^\dagger c_{j, \sigma} + \text{h.c.} + t_\perp \sum_i c_{i, T}^\dagger c_{i, B} + \text{h.c.} \\ & + U \sum_i n_{i, T} n_{i, B}. \end{aligned} \quad (1)$$

The operator c^\dagger (c) creates (annihilates) spin polarized fermions and the index $\sigma \in \{T, B\}$ labels the top and bottom layer of the heterostructure, see Fig. 1 a) for an illustration. Electrons are subject to a hopping term with strength t and an inter-layer tunnel coupling t_\perp . In AB stacking, one of the layers is rotated by 60° which exchanges the K and K' points. Due to spin-valley locking, this strongly suppresses t_\perp . In the following we analyse Eq. 1 and assume $t_\perp = 0$ throughout. We interpret elec-

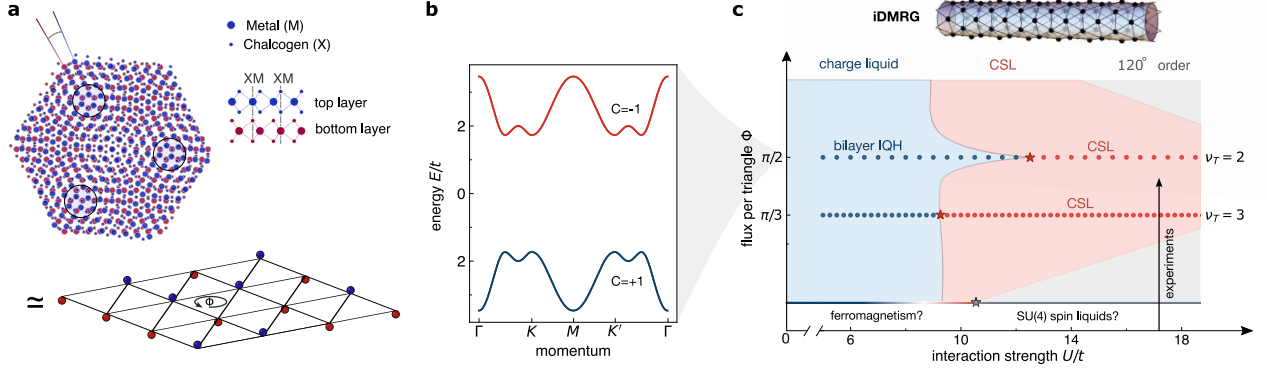


FIG. 1. **Setup and schematic phase diagram.** **a)** Twisted AB-stacked homobilayer TMD setup to realize a triangular Hubbard model. Top and bottom layers are drawn in blue and red. Electrons with pseudo-spin up (down) in the effective Hubbard model are depicted as blue (red) spheres in the bottom panel. **b)** Typical topological band structure of the Hofstadter model at $\pi/2$ flux and vanishing interactions. **c)** Schematic phase diagram of the half-filled triangular Hubbard model as a function of flux and interactions. Circles represent iDMRG data obtained on cylinders of circumference $L_y = 6$ and stars mark phase transitions. Remarkably, for intermediate to large interactions the dominant fraction of the phase diagram is a Chiral Spin Liquid (CSL). For weak interactions, the magnetic flux gives rise to a large variety of Hofstadter states, which can directly transition to the CSL.

trons in the top (bottom) layer as having pseudo spin $+1/2$ ($-1/2$). The magnetic field does not couple directly to the pseudo-spin, and its only effect is the generation of Peierls phases ϕ_{ij} .

Hamiltonian 1 then describes lattice versions of quantum Hall systems, which give rise to a large variety of phases. In the absence of interactions the system realizes a Hofstadter model that hosts a multitude of topologically non-trivial electronic bands which are induced by the magnetic field; see Fig. 1 b) for an example. As solid state systems are generically interacting, it is crucial to study the fate of these bands once electron repulsion is considered. While some states directly connect to the Hofstadter model at $U = 0$, interactions can also stabilize exotic phases of matter. One such example are excitonic superfluids, which arise when pseudo-spin symmetry is broken spontaneously by the interactions. Another, even more exciting possibility, is the formation of states with intrinsic topological order, such as fractional Chern insulators. As opposed to integer Chern insulators which are understood in terms of free fermion models, fractional ones feature emergent gauge fields, anyonic excitations and long-range entanglement [22, 23].

As correlated insulating phases give rise to particularly interesting spin physics, we consider a single electron per moiré unit cell $n_e = 1$ from now on. This allows the system to become Mott insulating for strong enough interactions, which is the natural regime for TMDs [24–26]. This limit is understood by eliminating the doubly occupied subspace with a Schrieffer-Wolff transformation [17],

leading to the following effective Hamiltonian

$$\begin{aligned} \hat{H}_{\text{eff.}} = & \frac{1}{U} \sum_{ij, \sigma \sigma'} t_{ij} t_{ji} (c_{i\sigma}^\dagger c_{i\sigma'}) (c_{j\sigma'}^\dagger c_{j\sigma}) \\ & - \frac{2}{U^2} \sum t_{ij} t_{jk} t_{ki} (c_{i\sigma}^\dagger c_{i\beta}) (c_{j\beta}^\dagger c_{k\alpha}) (c_{j\alpha}^\dagger c_{j\sigma}) \\ & + \mathcal{O}(t^4/U^3), \end{aligned} \quad (2)$$

which is equivalent to an effective spin system

$$\begin{aligned} \hat{H}_{\text{eff.}} = & J_H \sum_{\langle ij \rangle} \mathbf{S}_i \cdot \mathbf{S}_j + J_\chi \sum \mathbf{S}_i \cdot (\mathbf{S}_j \times \mathbf{S}_k) \\ & + \mathcal{O}(t^4/U^3), \end{aligned} \quad (3)$$

with anti-ferromagnetic Heisenberg interactions J_H and a chiral spin coupling J_χ . The couplings are related to the Hofstadter-Hubbard model parameters as follows

$$J_H = 2t^2/U, \quad J_\chi = 24 \sin(\Phi) t^3/U^2, \quad (4)$$

where Φ is the magnetic flux per triangle, which is given by $\phi_{ij} + \phi_{jk} + \phi_{ki}$ if i, j, k label sites on a single triangle.

Although the triangular lattice is frustrated, the ground state of the pure Heisenberg model, obtained for $U = \infty$, is a co-planar 120 degree (pseudo-) magnet [27, 28]. However, when interactions are lowered or the magnetic flux is increased, the ground state of the fermion system is still a subject of debate. We will show that J_χ can melt the 120 degree order and give way to an exceptionally stable CSL. The hallmark of this exotic phase is a fractionalization of the spins into spinons f_α , which is captured by a parton ansatz $\vec{S} = \frac{1}{2} \sum_{\alpha, \beta=0}^1 f_\alpha^\dagger \vec{\sigma}_{\alpha\beta} f_\beta$. Expressing Eq. 3 in terms of the spinons leads to a Hamiltonian, identical to Eq. 2 with electrons replaced by the spinons. The price to pay

in this representation is a single occupancy constraint $\sum_{\alpha} f_{i,\alpha}^{\dagger} f_{i,\alpha} = 1$ which must be imposed on each site i . This is similar to the Schrieffer-Wolff construction in Eq. 2, where we projected out double occupancies to describe the Mott insulator. Spinons evolving with Eq. 2 can only hop in a correlated fashion, and remain confined for conventional magnetic phases such as the 120 degree order. The spin liquid phase differs from conventional magnets by the absence of long-range order and self-consistently generated hopping terms $\langle f_{i,\alpha}^{\dagger} f_{j,\alpha} \rangle \neq 0$, necessary for fractionalization. The generation of such currents is an indication for the formation of singlets and a mean-field decoupling around such configurations leads to simple trial Hamiltonians:

$$H_{\text{trial}} = \sum_{\langle ij \rangle, \alpha} \tilde{t}_{ij} f_{i\alpha}^{\dagger} f_{j\alpha}. \quad (5)$$

The CSL arises when the (self-consistently determined) hopping matrix \tilde{t}_{ij} generates topological Chern bands, which are fully filled by the spinons. The single occupancy constraint then gives the spinons anyonic character [1, 17]. Despite being a potentially fragile phase at zero flux, we will show that magnetic fields strongly favor the formation of the CSL, see Fig. 1 c) for a schematic phase diagram.

While this discussion assumed strong magnetic fields to fully polarize the electronic spin, we point out that rich physics also arises when Zeeman splittings are small. Then, the system has additional (approximate) symmetries which have been proposed to give rise to more exotic SU(4) spin liquids [12]. How this and other phases interplay with the Hofstadter states is an interesting open question, which is beyond the scope of this work.

Furthermore our discussion based on the effective spin model neglects higher order ring-exchange processes, which become increasingly important close to the Mott transition. In order to fully capture the properties of the system, we instead study the electronic Hamiltonian of Eq. 1 directly, without projecting out the higher energy subspace [29]. In the following, we emphasize the rich physics of the model by studying a subset of phase transitions from Hofstadter states to the CSL.

Phases of the pseudo-spin Hofstadter-Hubbard model at specific flux.— We consider in detail the half-filled triangular Hubbard model deep inside the Hofstadter butterfly regime with two fluxes $\Phi \in \{\pi/3, \pi/2\}$. These flux values correspond to total filling factors of $\nu_T = 2\pi n_e / 2\Phi \in \{3, 2\}$, where 2Φ is the flux per unit cell and n_e is the number of electrons per unit cell ($n_e = 1$ at half-filling, which is what we consider throughout this work). For these flux values various exotic phases of matter can be stabilized. For example, at weak interactions the system could realize gapped bilayer integer quantum Hall (IQH) and gapless excitonic insulators, respectively. For large interactions, these phases compete with magnetic ordering and exotic spin liquids. Given the insights

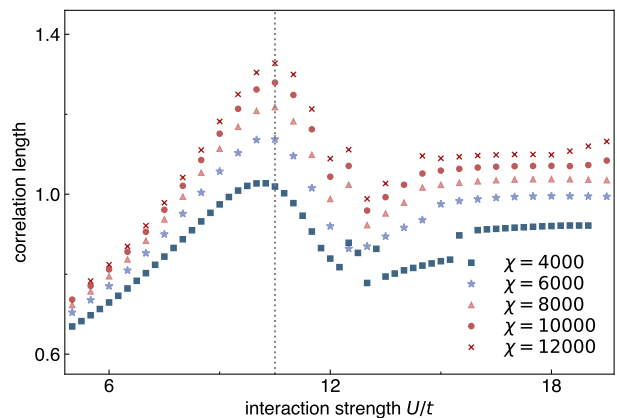


FIG. 2. **Ground state correlation length for $\Phi = \pi/2$.** We show the correlation length in the charge sector $(S_z, Q, k_y) = (0, 0, 0)$ as a function of U/t for different values of the bond dimension χ . Around $U \simeq 10.5t$ the correlation length grows with bond dimension, which is indicative of phase transition melting the bilayer quantum Hall state. The dotted grey line serves as a guide to the eye.

from the effective spin model in Eq. 3 the precise value of the external flux only determines the ratio of J_{χ}/J_H in the Mott insulator. However, in the quantum Hall regime its value is essential, as it determines charge gap. In order to determine which phases are stabilized by the microscopic Hofstadter-Hubbard model, we resort to numerical methods.

Studying fermions in magnetic fields poses a significant numerical challenge. Here, we use matrix product states (MPS) to obtain an unbiased variational approximation of the many-body wave function. This Ansatz allows for an expansion in terms of the entanglement, that is controlled by the maximal bond dimension χ of the MPS. If both the quantum Hall states and the CSL are gapped, they can be efficiently represented in terms of an MPS on a cylindrical lattice, that is finite in one direction but infinite in the other, because the total amount of entanglement is finite for such lattice geometries. This method has been successfully applied to phases with intrinsic topological order, which lead to a better understanding of fractional quantum Hall (FQH) and fractional Chern insulators; see e.g. [30–32]. We variationally optimize the MPS by infinite Density Matrix Renormalization Group (iDMRG), implemented via the TeNPy library [33]. Since the bond dimension, and hence the numerical costs, grow exponentially with the cylinder circumference, in this work we focus on $L_y = 6$, which fits both fluxes $\Phi = \pi/2, \pi/3$ with periodic boundary conditions.

Working in the infinite limit along the x-direction, we can directly obtain the correlation functions as well as the correlation length from the transfer matrix of the corresponding MPS unit cell. We use these methods to deter-

mine the ground-state phase diagram of the Hofstadter-Hubbard model given by Eq. 1. Even though the precise points of the phase transitions may shift depending on the cylinder circumference, we expect the structure of the phase diagram to be similar in the two dimensional limit [29]. To be able to perform the simulations with high bond dimensions and therefore small truncation errors, we utilize the $U(1) \times U(1)$ symmetries generated by the z-component of pseudo spin $\sum_i S_i^z = \sum_i \hat{n}_i^T - \hat{n}_i^B$ and particle conservation $\sum_i \hat{n}_i^T + \hat{n}_i^B$ as well as translation symmetry along the y-direction [34, 35], which determine the S_z , Q , and k_y quantum numbers, respectively.

Quantum phase transition at $\Phi = \pi/2$.— For $\Phi = \pi/2$ flux per triangle and small U/t the system is in a bilayer IQH state, defined by a fully filled topological band with Chern number $C = 1$ for each pseudo spin, see Fig. 1b). We find signatures of a phase transition by studying the ground state correlation length as a function of interactions U/t , which is shown for operators carrying the quantum numbers $(S_z, Q, k_y) = (0, 0, 0)$ in Fig. 2. As interactions are increased, the correlation length grows significantly with bond dimension around a critical interaction strength of $U_c \sim 10.5t$, which indicates a gap closing phase transition. In contrast to the bilayer IQH state, identifying the phases for $U > U_c$ is more subtle. The most relevant competing states are 120 degree spin-order, tetrahedral spin-order, excitonic insulators, and the chiral spin liquid.

We shed light on the large U phase by noticing that the enhanced correlation length is accompanied by a simultaneous reorganization of the half-cylinder entanglement spectrum, shown in Fig. 3 (a,b). The entanglement spectrum directly encodes the energy levels of the edge theory on a half-infinite cylinder, which are distinct for the bilayer IQH and the other candidate phases. The edge theory of the bilayer IQH for small U/t is given by two chiral modes, one for each layer. Their excitations are understood as follows: For $k_y = 0$ there is a unique state where neither of the edge modes is excited, leading to a single dominant entanglement eigenvalue. To create a momentum $k_y = 1 \cdot 2\pi/L_y$ excitation, one can shift the lowest lying electron by one momentum quanta, and promote it to the state just above the Fermi level. As this can be done in both layers, we find two such excitations, leading to two entanglement eigenvalues. In the appropriate basis these excitations decouple completely and correspond to total-density and spin-density wave excitations. Continuing this counting, one finds that the momentum resolved entanglement spectrum for increasing momenta k_y is given by $(1, 2, 5, 10, \dots)$ entanglement eigenvalues in each spin sector, see Fig. 3 a). These density- and spin-wave modes are arranged in a representation of an underlying $U(1) \otimes SU(2)_1$ algebra, as expected for the boundary of a double copy of an IQH state. For $U > U_c$, on the other hand, the ground state loses several edge excitations; see Fig. 3 b). This is natural once the sys-

tem turns Mott insulating, at which point density waves acquire a finite energy cost. The spectrum then consists only of spin waves described by a representation of the $SU(2)_1$ algebra, which leads to a $(1, 1, 2, 3, 5, \dots)$ counting. The edge is therefore captured by a chiral $SU(2)_1$ Wess-Zumino-Witten model, which matches the edge theory of the chiral spin liquid [36, 37].

We further analyse the topological character of the bilayer IQH and the suspected CSL by inserting fluxes through our cylinder, which realizes Laughlins charge pump [38]. The IQH state responds to the insertion of 2π magnetic flux by transferring a single charge from one end of the cylinder to the other in each layer, illustrated in Fig 3 c) (red markers). To couple to the charge-neutral spin edge modes, one has to thread opposite fluxes in the two layers. The IQH state then pumps one electron in the top and one hole in the bottom layer each carrying a spin of $1/2$, leading to a pseudo-spin transfer of unity, see Fig 3 c) (blue markers). Combining these results, we infer that the excitations carry both charge and spin.

For $U > U_c$ the system no longer pumps electric charge when threading magnetic fluxes, consistent with a Mott insulating state. However, it still exhibits quantized spin transfer for oppositely inserted fluxes, see panel d) of Fig. 3. Inserting π flux for the electrons corresponds to a 2π flux insertion in the effective spin Hamiltonian Eq. 3. From this point of view we pump a single spin after threading 4π spin-flux, realizing a fractional spin Hall effect. This can be intuitively understood via the Kalmeyer-Laughlin construction, where the spin system is mapped to a half-filled Bose-Hubbard model in the presence of a fictitious background magnetic field [15]. Our observed spin pumping is then explained by the formation of a $\nu = 1/2$ bosonic FQH state which is identified as the chiral spin liquid in the spin picture. The same conclusion can be reached starting from a purely fermionic model, although the discussion is more involved [1]. The fractional spin-Hall effect and the absence of charge transport therefore serves as a direct signature of a fractional Hall state for spin. Putting these findings together we identify the phase into which the bilayer IQH phase transitions when increasing interactions to $U > U_c$ as a CSL.

Surprisingly, we do not find intermediate tetrahedrally ordered magnets, which were predicted to appear in the effective spin model of Eq. 3. This suggests a direct transition between a state with topological bands and a state with genuine topological order when keeping the original fermionic degrees of freedom.

We also remark that the CSL hosts two degenerate ground states in the thermodynamic limit, i.e., for $L_x, L_y = \infty$, which reside in the $k_y = 0$ and $k_y = \pi$ momentum sectors. In our geometry, the ground state energies in these sectors approach each other and cross shortly after the transition, which is a finite size effect of our simulations [18, 29].

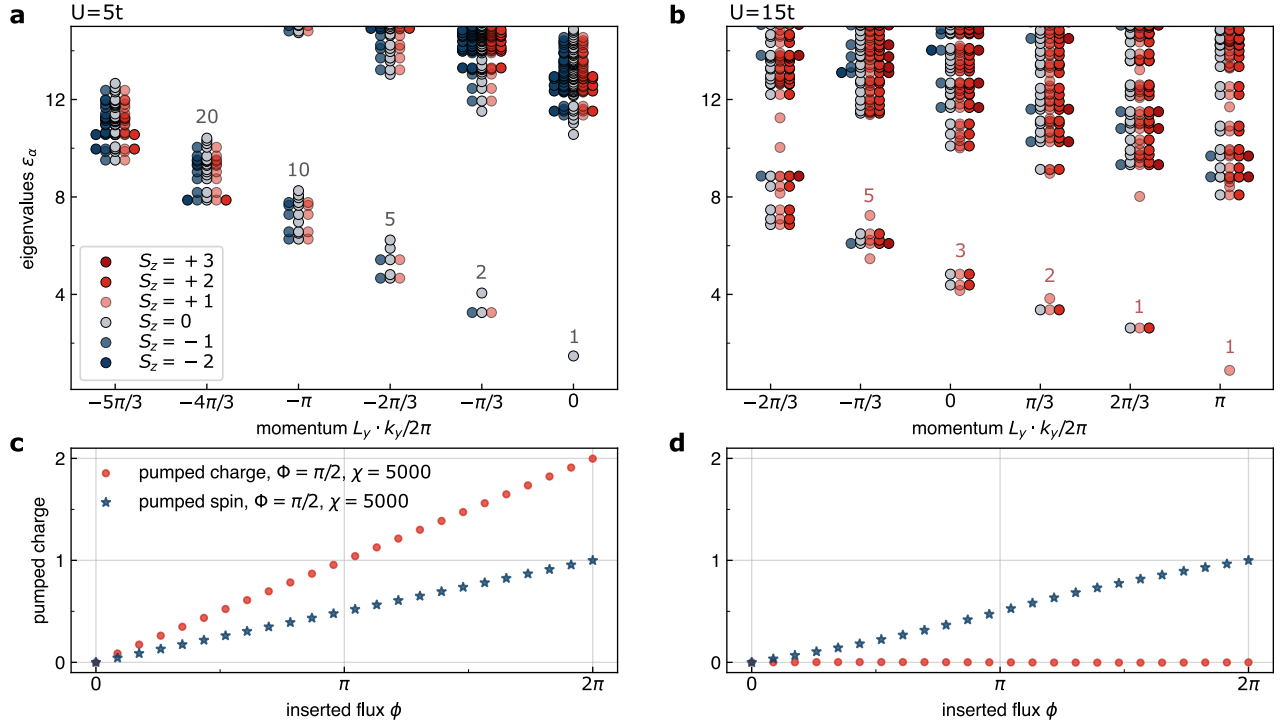


FIG. 3. **Topological properties for $\Phi = \pi/2$.** Edge properties and charge pumping for $\Phi = \pi/2$ for $U = 5t$ (a,c) and $U = 15t$ (b,d). **a)** Ground state entanglement spectrum in the IQH phase for $\chi = 10000$ and charge $Q = 0$. The spectrum obeys a (1,2,5,10,...) counting rule characteristic for an edge theory of two chiral bosons, which suggests an IQH state in both the top and bottom layer. **b)** Ground state entanglement spectrum in the CSL for $\chi = 10000$ and charge $Q = 0$. The spectrum obeys the (1,1,2,3,5,...) counting rule for the edge theory of the CSL phase. **(c,d)** Pumped charge under flux insertion through the cylinder. Red and blue dots indicate flux that is inserted equally and oppositely in the two layers. While the pumping in **c)** is a direct consequence of two charge-carrying edge modes of the bilayer IQH state, the charge pumping in the CSL regime **d)** vanishes entirely, consistent with the separation of spin and charge degrees of freedom while the spin remains quantized.

Competition between Hall states and spin liquids at $\Phi = \pi/3$.— For $\nu_T = 3$, we no longer expect a quantized Hall conductance as the Landau bands are partially filled. This opens the possibilities for other charge liquids, such as excitonic superfluids. Here, we choose unit cells of size $L_x = 3$, which allows us to reliably prepare states with fixed momenta along the y-direction [39].

We find that for small U/t the system does not exhibit any quantized pumping; see supplementary materials [39]. Although it is suggested by the continuum limit, we do not find long range ferromagnetic correlations of the Hall liquid, which may be a feature of the Hofstadter-Hubbard model at half filling. While we cannot uniquely identify the nature of this state, its response is consistent with a featureless Hall state [40]. However, once interactions are raised a sharp transition occurs around $U \simeq 8.5t$, as evidenced by the growing correlation length; see Fig. 4.

We find that the transition (on finite cylinders) occurs in steps: First, for small U/t the ground state is found at zero momentum. As U increases the correlation length in the $k_y = \pi$ sector diverges. Then, quickly after this divergence the $k_y = \pi$ state becomes the new ground state

of the system. Afterwards the energy splitting between the two states remains roughly constant [39].

There are several possible candidate states once the system becomes insulating. Following the analysis of the previous section we can identify the phase for $U \geq 8.5t$ as a CSL [39]. In particular, the state exhibits a fractional spin-Hall effect and shows the characteristic half-cylinder entanglement spectra. Although the $k_y = 0$ state is higher in energy than the $k_y = \pi$ state for $U \geq 8.5t$, the edge theories of both states are in good agreement with the $SU(2)_1$ WZW model describing the boundary of the CSL.

While the robust spin liquid is a universal feature of the large U phase for both fluxes, the charge to spin liquid transitions are clearly distinct for $\nu_T = 2$ and $\nu_T = 3$. Most notably for $\nu_T = 3$ the CSL appears already for much weaker interactions compared to $\nu_T = 2$. This indicates that the charge liquid at $\nu_T = 3$ is less stable, than the $\nu_T = 2$ bilayer IQH state. This behaviour is reminiscent of the competition between Wigner crystals and Hall states in electron gases, where integer and fractional quantum Hall states extend further into the gapped crystalline phase than their gapless counterparts [26, 41].

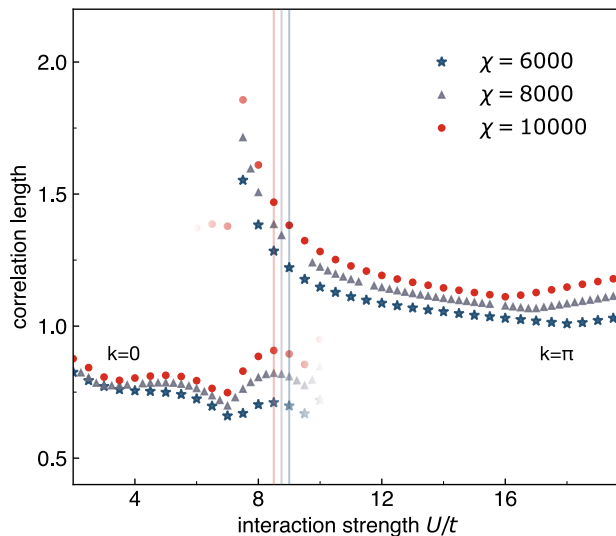


FIG. 4. **Transition for $\Phi = \pi/3$.** The ground state correlation length for operators in the sector $(S_z, Q, k_y) = (0, 0, 0)$. In the lowest energy $k_y = \pi$ state, the correlation length strongly increases around $U \simeq 8.5t$, indicating a sharp transition to a chiral spin liquid. The energy crossing of the $k = 0$ and $k = \pi$ states is indicated by the vertical lines and is a finite size effect. The two momentum states are expected to be the degenerate ground states of the CSL in the thermodynamic limit.

Signatures of layer pseudo spin.— Potentially the biggest challenge in spin-liquid physics is to find experimental signatures for their existence. Many of the previously proposed detection schemes of electronic-spin liquid states—such as a quantum thermal Hall effect—are readily generalized to layer-spin systems. However layer pseudo-spin has the additional advantage of being easier to manipulate and probe. Consequently one can start to think about completely novel detection schemes unique to the layer degree of freedom. One such example are counterflow measurements, which exhibit a quantized Hall response and arguably provide the most convincing evidence for the existence of a chiral layer-pseudo-spin liquid state [12]. Sample inhomogeneity and the difficulty in electrical isolation of the two layers render such a measurement rather demanding.

Nevertheless, additional evidence for a CSL state could be obtained using all-optical measurements, which overcome several obstacles through tight focusing of the probe lasers into regions where the moiré potential is uniform. An optical characterization could start by measuring the spin-susceptibility at finite field E_z , which acts as an effective magnetic field for pseudo spins, as a function of temperature: since each layer generically has a different exciton resonance¹, measuring the attractive

polaron resonance strength of each layer directly yields the pseudo-spin magnetization $\langle S_z \rangle$. The spin susceptibility should increase as T is lowered towards the spin gap Δ_s/k_B , but would show exponential suppression for $k_B T < \Delta_s$. Similarly, measurement of magnetization as a function of E_z at low temperatures $k_B T \ll \Delta_s$ should show the existence of a spin-gap. In experiments the external magnetic field $B_z = 0$ limit realizes a magnetically ordered state with gapless spin excitations for a large range of U/t . As the magnetic field is increased, one can therefore directly measure the opening of the spin gap, see also Fig. 1c). The appearance of the charge gap in turn, is evidenced by the cusps in attractive and repulsive polaron resonances, indicating the modification of dynamical screening of excitons by electrons. This allows us to identify stable spin liquids by monitoring the charge gap as a function of carrier doping. If small enough interactions can be reached experimentally, this also enables the identification of Hofstadter states.

Complementary insights could be obtained by measuring $\langle S_{\mathbf{q}=0}^z(t) S_{\mathbf{q}=0}^z(0) \rangle$ using correlations between resonantly scattered photons on the attractive polaron resonance. Hanbury Brown & Twiss type photon correlation measurements would yield diverging fluctuations close to a critical point and should allow for determination of dynamical critical exponents. If coherent optical Raman manipulation of layer pseudo-spin is possible, then suppression of spin noise along all axes for $k_B T \ll \Delta_s$ can be measured [42]. Further, direct evidence for the emergence of a gauge field could be verified using optical Hall measurements. It has been demonstrated that effective electric fields can be imprinted on excitons using crossed magnetic and time dependent electric fields [43]. A combination of such an effective dipole electric field and the emergent gauge field should result in layer-contrasting Hall effect [44], which can be measured by determining the spatial dependence of the attractive polaron resonance in each layer along the axis that is orthogonal to the dipole electric field. Furthermore, novel momentum-resolved techniques unique to 2D materials could also allow for the measurement of ARPES-like spectra [45] which can provide signatures of spinon excitations in quantum spin liquids [46].

Due to the geometric frustration, several ordered phases are close in energy to the spin liquid and which of those states is selected as ground state is a non-trivial question. In experiments it is therefore crucial to identify ordered states in proximity to the CSL. Most importantly, the dominant competing phase close to the Mott transition—tetrahedral magnetic order—can be identified either by direct imaging with STM spectroscopy [24], or probed optically by Bragg scattering of intra-layer excitons [47, 48]. Such local probes are particularly relevant

¹ This is true also for twisted homobilayer structures where strain

lifts the degeneracy of the exciton resonance

for near term devices as they are readily accessible and largely insensitive to large-scale disorder.

Conclusions and Outlook.— We have shown how a large class of quantum phases and transitions can be studied in multi-layer TMDs. In particular, topologically ordered CSLs can be stabilized by utilizing the layer degree of freedom as a synthetic spin [7, 12]. The absence of a magnetic Zeeman effect for the pseudo-spin allows us to target topological states by controlling the strength of ring exchange processes using large external magnetic fields. For weak interactions a variety of Hofstadter states can be prepared by sweeping B_z , while a CSL forms for intermediate interaction strengths. The field induced CSL is found to be exceptionally robust and occupies a large region of the phase diagram. Combined with the electric tunability and layer-selective read-out of layer pseudo-spin, this makes TMD heterostructures particularly promising platforms to study spin liquid physics. Novel probing schemes unique to the pseudo-spin degree of freedom offer an additional advantage of these systems over conventional spin liquid candidates. Competing spin and charge ordered phases can be more easily identified; while counterflow measurements [12] directly probe the topology of the spin liquid. It is also possible to find fingerprints of the spin liquid phase with all optical measurements, which provide local probes that are crucial for near-term devices.

Our results open up several theoretical and experimental avenues to study topological order and exotic phase transitions. For one, Mott insulators can be stabilized at fractional fillings by longer-ranged interactions, leading to spin systems with different lattice geometries and more exotic states for small interaction strengths. More specifically, for $\Phi = \pi/3$ densities of $n_e = 1/3, 1/9, \dots$ realize excitonic insulator candidates and FQH states respectively, both of which eventually transition to frustrated spin states in Mott-Wigner insulators at large U/t . This poses interesting questions about the nature of quantum phase transitions between topological order in the charge and spin sectors. Furthermore, in the weak field limit a variety of interesting competing states emerges, and their interplay is largely unexplored. Most notably, this regime is expected to feature Hofstadter physics, quantum Hall ferromagnetism and $SU(4)$ spin liquids [12].

Acknowledgments.— We thank M. Drescher, K. Fai Mak, J. Feldmeier, J. Hauschild, F. Pollmann, J. Shan, T. Smolenski, and A. Young for fruitful discussions. We acknowledge support from the Deutsche Forschungsgemeinschaft (DFG, German Research Foundation) under Germany's Excellence Strategy-EXC-2111-390814868 and DFG grant No. KN1254/2-1, No. KN1254/1-2, the European Research Council (ERC) under the European Union's Horizon 2020 research and innovation programme (grant agreement No. 851161), as well as the Munich Quantum Valley, which is supported by the Bavarian state government with funds from the Hightech

Agenda Bayern Plus. The work at ETH Zurich was supported by the Swiss National Science Foundation (SNSF) under Grant Number 200021-204076.

Data and materials availability.— Data analysis and simulation codes are available on Zenodo upon reasonable request [49].

-
- [1] X.-G. Wen, *Quantum Field Theory of Many-Body Systems: From the Origin of Sound to an Origin of Light and Electrons*, Oxford Graduate Texts (Oxford University Press, Oxford, 2007).
 - [2] L. Savary and L. Balents, Quantum spin liquids: a review, *Reports on Progress in Physics* **80**, 016502 (2016).
 - [3] J. Knolle and R. Moessner, A field guide to spin liquids, *Annual Review of Condensed Matter Physics* **10**, 451 (2019), <https://doi.org/10.1146/annurev-conmatphys-031218-013401>.
 - [4] J. G. Rau, E. K.-H. Lee, and H.-Y. Kee, Spin-orbit physics giving rise to novel phases in correlated systems: Iridates and related materials, *Annual Review of Condensed Matter Physics* **7**, 195 (2016), <https://doi.org/10.1146/annurev-conmatphys-031115-011319>.
 - [5] J. P. Eisenstein, G. S. Boebinger, L. N. Pfeiffer, K. W. West, and S. He, New fractional quantum hall state in double-layer two-dimensional electron systems, *Phys. Rev. Lett.* **68**, 1383 (1992).
 - [6] X. Liu, K. Watanabe, T. Taniguchi, B. I. Halperin, and P. Kim, Quantum hall drag of exciton condensate in graphene, *Nature Physics* **13**, 746 (2017).
 - [7] I. Schwartz, Y. Shimazaki, C. Kuhlenskamp, K. Watanabe, T. Taniguchi, M. Kroner, and A. Imamoglu, Electrically tunable feshbach resonances in twisted bilayer semiconductors, *Science* **374**, 336 (2021), <https://www.science.org/doi/pdf/10.1126/science.abj3831>.
 - [8] E. C. Regan, D. Wang, C. Jin, M. I. Bakti Utama, B. Gao, X. Wei, S. Zhao, W. Zhao, Z. Zhang, K. Yumigeta, M. Blei, J. D. Carlström, K. Watanabe, T. Taniguchi, S. Tongay, M. Crommie, A. Zettl, and F. Wang, Mott and generalized Wigner crystal states in WSe₂/WS₂ moiré superlattices, *Nature* **579**, 359 (2020).
 - [9] Y. Shimazaki, I. Schwartz, K. Watanabe, T. Taniguchi, M. Kroner, and A. Imamoglu, Strongly correlated electrons and hybrid excitons in a moiré heterostructure, *Nature* **580**, 472 (2020).
 - [10] Y. Tang, L. Li, T. Li, Y. Xu, S. Liu, K. Barmak, K. Watanabe, T. Taniguchi, A. H. MacDonald, J. Shan, and K. F. Mak, Simulation of Hubbard model physics in WSe₂/WS₂ moiré superlattices, *Nature* **579**, 353 (2020).
 - [11] Y. Zhou, D. N. Sheng, and E.-A. Kim, Quantum phases of transition metal dichalcogenide moiré systems, *Phys. Rev. Lett.* **128**, 157602 (2022).
 - [12] Y.-H. Zhang, D. N. Sheng, and A. Vishwanath, Su(4) chiral spin liquid, exciton supersolid, and electric detection in moiré bilayers, *Phys. Rev. Lett.* **127**, 247701 (2021).
 - [13] D. R. Hofstadter, Energy levels and wave functions of bloch electrons in rational and irrational magnetic fields, *Phys. Rev. B* **14**, 2239 (1976).
 - [14] P. Anderson, Resonating valence bonds: A new kind of insulator?, *Materials Research Bulletin* **8**, 153 (1973).

- [15] V. Kalmeyer and R. B. Laughlin, Equivalence of the resonating-valence-bond and fractional quantum hall states, *Phys. Rev. Lett.* **59**, 2095 (1987).
- [16] X. G. Wen, F. Wilczek, and A. Zee, Chiral spin states and superconductivity, *Phys. Rev. B* **39**, 11413 (1989).
- [17] O. I. Motrunich, Orbital magnetic field effects in spin liquid with spinon fermi sea: Possible application to $\kappa-(\text{ET})_2\text{Cu}_2(\text{CN})_3$, *Phys. Rev. B* **73**, 155115 (2006).
- [18] S.-S. Gong, W. Zhu, J.-X. Zhu, D. N. Sheng, and K. Yang, Global phase diagram and quantum spin liquids in a spin- $\frac{1}{2}$ triangular antiferromagnet, *Phys. Rev. B* **96**, 075116 (2017).
- [19] L. A. Ponomarenko, R. V. Gorbachev, G. L. Yu, D. C. Elias, R. Jalil, A. A. Patel, A. Mishchenko, A. S. Mayorov, C. R. Woods, J. R. Wallbank, M. Mucha-Kruczynski, B. A. Piot, M. Potemski, I. V. Grigorieva, K. S. Novoselov, F. Guinea, V. I. Fal'ko, and A. K. Geim, Cloning of dirac fermions in graphene superlattices, *Nature* **497**, 594 (2013).
- [20] Y. Tang, K. Su, L. Li, Y. Xu, S. Liu, K. Watanabe, T. Taniguchi, J. Hone, C.-M. Jian, C. Xu, K. F. Mak, and J. Shan, *Frustrated magnetic interactions in a wigner-mott insulator* (2022).
- [21] N. C. Hu and A. H. MacDonald, Competing magnetic states in transition metal dichalcogenide moiré materials, *Phys. Rev. B* **104**, 214403 (2021).
- [22] X. G. WEN, Topological orders in rigid states, *International Journal of Modern Physics B* **04**, 239 (1990), <https://doi.org/10.1142/S0217979290000139>.
- [23] M. Levin and X.-G. Wen, Detecting topological order in a ground state wave function, *Phys. Rev. Lett.* **96**, 110405 (2006).
- [24] H. Li, S. Li, E. C. Regan, D. Wang, W. Zhao, S. Kahn, K. Yumigeta, M. Blei, T. Taniguchi, K. Watanabe, S. Tongay, A. Zettl, M. F. Crommie, and F. Wang, Imaging two-dimensional generalized wigner crystals, *Nature* **597**, 650 (2021).
- [25] Y. Zhou, J. Sung, E. Brutschea, I. Esterlis, Y. Wang, G. Scuri, R. J. Gelly, H. Heo, T. Taniguchi, K. Watanabe, G. Záránd, M. D. Lukin, P. Kim, E. Demler, and H. Park, Bilayer wigner crystals in a transition metal dichalcogenide heterostructure, *Nature* **595**, 48 (2021).
- [26] T. Smoleński, P. E. Dolgirev, C. Kuhlenskamp, A. Popert, Y. Shimazaki, P. Back, X. Lu, M. Kroner, K. Watanabe, T. Taniguchi, and et al., Signatures of wigner crystal of electrons in a monolayer semiconductor, *Nature* **595**, 53–57 (2021).
- [27] S. Miyashita, A variational study of the ground state of frustrated quantum spin models, *Journal of the Physical Society of Japan* **53**, 44 (1984), <https://doi.org/10.1143/JPSJ.53.44>.
- [28] D. A. Huse and V. Elser, Simple variational wave functions for two-dimensional heisenberg spin- $\frac{1}{2}$ antiferromagnets, *Phys. Rev. Lett.* **60**, 2531 (1988).
- [29] A. Szasz, J. Motruk, M. P. Zaletel, and J. E. Moore, Chiral spin liquid phase of the triangular lattice hubbard model: A density matrix renormalization group study, *Phys. Rev. X* **10**, 021042 (2020).
- [30] M. P. Zaletel, R. S. K. Mong, F. Pollmann, and E. H. Rezayi, Infinite density matrix renormalization group for multicomponent quantum hall systems, *Phys. Rev. B* **91**, 045115 (2015).
- [31] A. G. Grushin, J. Motruk, M. P. Zaletel, and F. Pollmann, Characterization and stability of a fermionic $\nu = 1/3$ fractional chern insulator, *Phys. Rev. B* **91**, 035136 (2015).
- [32] P. Kumar and F. D. M. Haldane, Neutral excitations of quantum hall states: A density matrix renormalization group study, *Phys. Rev. B* **106**, 075116 (2022).
- [33] J. Hauschild and F. Pollmann, Efficient numerical simulations with Tensor Networks: Tensor Network Python (TeNPy), *SciPost Phys. Lect. Notes*, 5 (2018), code available from <https://github.com/tenpy/tenpy>.
- [34] J. Motruk, M. P. Zaletel, R. S. K. Mong, and F. Pollmann, Density matrix renormalization group on a cylinder in mixed real and momentum space, *Physical Review B* **93**, 155139 (2016).
- [35] G. Ehlers, S. R. White, and R. M. Noack, Hybrid-space density matrix renormalization group study of the doped two-dimensional Hubbard model, *Physical Review B* **95**, 125125 (2017).
- [36] X. G. Wen, Gapless boundary excitations in the quantum Hall states and in the chiral spin states, *Phys. Rev. B* **43**, 11025 (1991).
- [37] J. E. Moore and F. D. M. Haldane, Edge excitations of the $\nu =$ spin-singlet quantum Hall state, *Phys. Rev. B* **55**, 7818 (1997).
- [38] R. B. Laughlin, Quantized hall conductivity in two dimensions, *Phys. Rev. B* **23**, 5632 (1981).
- [39] See supplementary online material.
- [40] J. Eisenstein, Exciton condensation in bilayer quantum hall systems, *Annual Review of Condensed Matter Physics* **5**, 159 (2014).
- [41] K. A. Villegas Rosales, S. K. Singh, M. K. Ma, M. S. Hossain, Y. J. Chung, L. N. Pfeiffer, K. W. West, K. W. Baldwin, and M. Shayegan, Competition between fractional quantum hall liquid and wigner solid at small fillings: Role of layer thickness and landau level mixing, *Phys. Rev. Research* **3**, 013181 (2021).
- [42] A. G. Salvador, A. Imamoğlu, and E. Demler, Private Communication (2022).
- [43] H.-T. Lim, E. Togan, M. Kroner, J. Miguel-Sanchez, and A. Imamoğlu, Electrically tunable artificial gauge potential for polaritons, *Nature Communications* **8**, 14540 (2017).
- [44] D. Zhai, C. Chen, C. Xiao, and W. Yao, *Layer-contrasted hall effect in twisted bilayers with time reversal symmetry* (2022).
- [45] A. Inbar, J. Birkbeck, J. Xiao, T. Taniguchi, K. Watanabe, B. Yan, Y. Oreg, A. Stern, E. Berg, and S. Ilani, *The quantum twisting microscope* (2022).
- [46] W. Kadow, L. Vanderstraeten, and M. Knap, Hole spectral function of a chiral spin liquid in the triangular lattice hubbard model, arXiv preprint arXiv:2202.03458 (2022).
- [47] Y. Shimazaki, C. Kuhlenskamp, I. Schwartz, T. Smoleński, K. Watanabe, T. Taniguchi, M. Kroner, R. Schmidt, M. Knap, and A. Imamoğlu, Optical signatures of periodic charge distribution in a mott-like correlated insulator state, *Phys. Rev. X* **11**, 021027 (2021).
- [48] A. G. Salvador, C. Kuhlenskamp, L. Ciorciaro, M. Knap, and A. Imamoğlu, Optical signatures of periodic magnetization: The moiré zeeman effect, *Phys. Rev. Lett.* **128**, 237401 (2022).
- [49] C. Kuhlenskamp, W. Kadow, A. Imamoğlu, and M. Knap, *Tunable topological order of pseudo spins in semiconductor heterostructures* (2022).

- [50] Y. Gannot, Y.-F. Jiang, and S. A. Kivelson, Hubbard ladders at small u revisited, [Phys. Rev. B **102**, 115136 \(2020\)](#).

Supplemental Material: Tunable topological order of pseudo spins in semiconductor heterostructures

Gauge choice for different flux values

To implement a static magnetic field on the triangular lattice we perform a Peierls substitution $t_{ij} \rightarrow t_{ij}e^{i\phi_{ij}}$, where the choice of phases ϕ_{ij} is not unique. To accommodate for the $\Phi = \pi/2, \pi/3$ flux per triangle and to keep translational invariance in y direction, we perform our simulations on unit cells of size $L_x = 2, 3$. In the main text we chose gauges leading to the phase patterns shown in Fig. S1. As any gauge choice breaks explicit translational invariance, we work with unit cells and cylinder geometries which are commensurate with the flux.

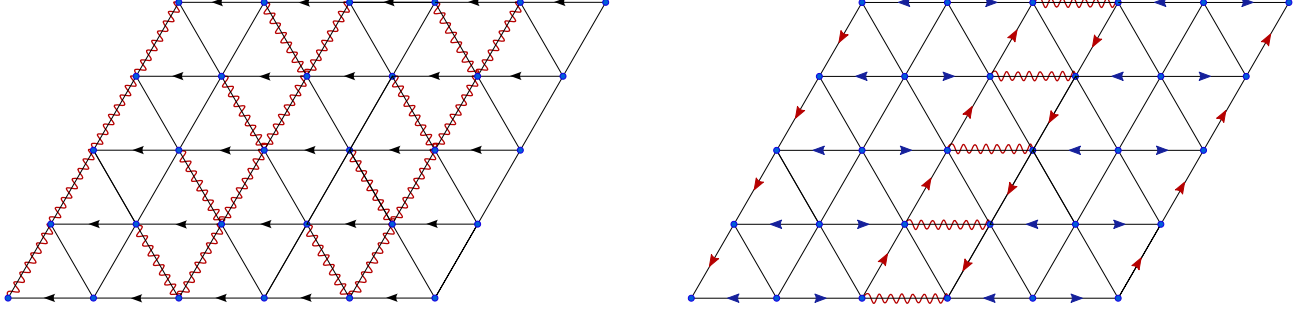


FIG. S1. **Gauge choices for different fluxes.** Flux patterns on the triangular lattice leading to $\Phi = \pi/2$ (a) and $\Phi = \pi/3$ (b). Hopping along a bond in the direction of a red (blue) arrow yields a phase factor of $e^{i2\pi/3}$ ($e^{i\pi/3}$), while hopping along a black arrow yields a phase of $e^{i\pi/2}$. Squiggly bonds carry a factor of -1 .

Ground state crossing for $\Phi = \pi/3$

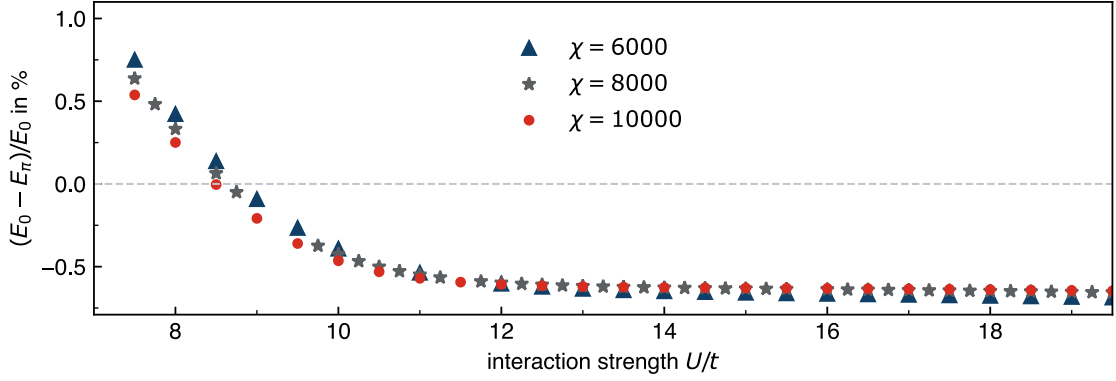


FIG. S2. **Energy difference of the lowest lying $k_y = 0$ and $k_y = \pi$ states for $\Phi = \pi/3$.** We find that for $U \simeq 8.5t$ the ground-state energies of the two momentum sectors cross. This point moves to weaker interactions as the bond dimension increases. This level crossing occurs in the vicinity of the enhanced correlation length observed in the main text. We expect that in the CSL phase both eigenstates are degenerate in the thermodynamic limit.

We can reliably prepare states in the $k_y = \pi$ and $k_y = 0$ sectors on the $L_x = 3$ unit cell and flux $\Phi = \pi/3$. As discussed in the main text, the two ground states of the CSL sectors lie at $k_y = 0, \pi$ but are slightly split due to finite size effects. Therefore, in our truncated system the transition from the Hall states to the CSL occurs in two steps: First the correlation length in the $k_y = \pi$ sector diverges and shortly thereafter its energy crosses with the $k_y = 0$ state and becomes the true finite-size ground state. We show the difference in ground state energies as a function of

interaction strength and bond dimension in Fig. S2. We find that the crossing takes places around $U \sim 8.75t$, where the correlation length of the $k_y = \pi$ state is still very large, as discussed in the main text.

Characterizing the phases for $\Phi = \pi/3$

While the precise value of the flux is important in the Hofstadter regime, as it determines the filling of the Chern bands, in the Mott insulating limit it simply controls the strength of the chiral spin term J_χ . Therefore, we generically expect chiral spin liquids to appear in the Mott insulator, as long as $J_\chi \sim \sin(\Phi)$ is large enough. Here we discuss the fate of the Mott insulator for $\Phi = \pi/3$, which corresponds to a filling of $\nu_T = 3$. Following the analysis done

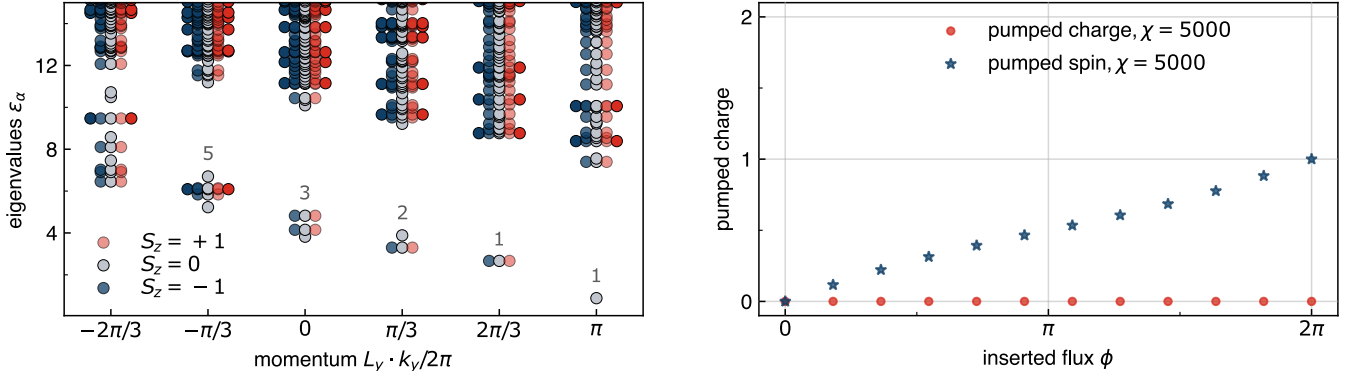


FIG. S3. **Entanglement spectrum and charge pumping for $\Phi = \pi/3$ and $U = 15t$.** Left panel: Entanglement spectrum for $\chi = 10000$. The symmetry resolved spectrum and its degeneracies agree with the $SU(2)_1$ WZW edge theory of the CSL. Right panel: The system pumps an integer pseudo spin under flux insertion, confirming the topological nature of the spinon bands.

for $\Phi = \pi/2$ in the main text, we compute the entanglement spectrum and analyze the pumped charges under flux insertion. Our results in the Mott limit are shown in Fig. S3 for $U = 15t$. The entanglement spectrum agrees with the spectrum of the $SU(2)_1$ WZW model describing the spin-density-wave excitations on the edge (left panel). The absence of gapless density-wave excitations, in addition to the vanishing pumped charge under the insertion of real magnetic flux (right panel) indicates that charges are frozen and hence that the state is insulating. Under the insertion of opposite fluxes in the two layers, i.e., when coupling to charge-neutral, spin excitations, we find a fractional spin Hall effect, as discussed in the main text [15, 29]. As expected, no charge is pumped under the insertion of opposite fluxes, and no spin is pumped under symmetric flux insertion (not shown). Hence, the state describes a CSL. These results demonstrate that the CSL is a generic feature of the Hofstadter-Hubbard model at strong coupling independent of the specific values of the magnetic field.

The fate of the Hofstadter states in the presence of weak interactions is a priori not obvious. For $\Phi = \pi/3$, we find that the system no longer exhibits quantized charge or spin pumping in the charge-liquid regime. To study the propensity of the state to develop long range order, we analyze spin, density and superconducting correlation functions, which are shown in Fig. S4. The formation of excitonic insulators and other layer-spin ordered states is ruled out, as we find exponentially decaying spin correlations, see Fig. S4 a). Similarly, density correlations show an initial exponential decay before saturating at a weak residual value of $\approx 10^{-4}$, which indicates weak charge order, shown in Fig. S4 b). Since this value is very small and the circumference of the cylinder is finite, we attribute this to finite size effects.

In the absence of magnetic fields, superconductivity has been discussed as a possible phase in the triangular Hubbard model [50]. The tendency to become superconducting is captured by the following pairing terms: $\hat{\Delta}(x, y) = (c_{T,x,y+1}^\dagger c_{B,x,y}^\dagger - c_{B,x,y+1}^\dagger c_{T,x,y}^\dagger)/\sqrt{2}$ and the corresponding correlation functions are depicted in Fig. S4 c). This shows that superconducting correlations are exponentially decaying and we do not find signatures of superconducting order. Our analysis therefore suggests that the $\Phi = \pi/3$ state in the half-filled triangular lattice is consistent with a featureless Hall state.

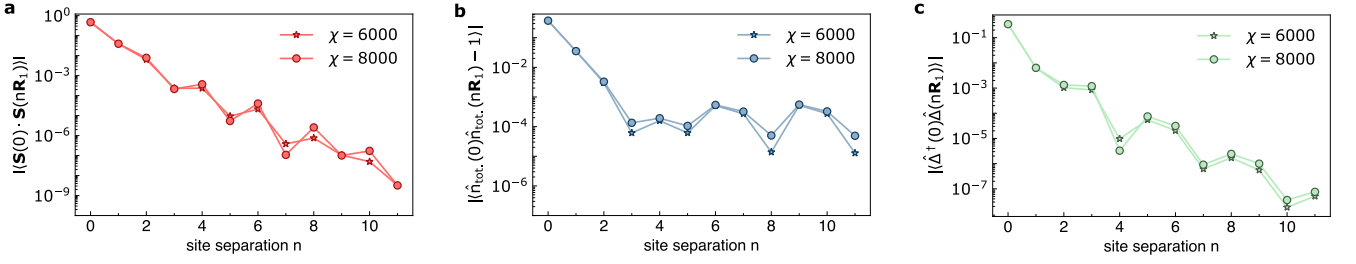


FIG. S4. **Correlations in the weakly interacting phase for $\Phi = \pi/3$.** Correlation functions are plotted for $U/t = 3$ as a function of distance along the x-direction. **a)** Spin-correlations are exponentially decaying, showing the absence of long-range spin order. **b)** Density correlations show an initial exponential decay and a weak residual tendency to form charge order. **c)** Superconducting correlations are small and decay exponentially. This indicates that the state may be a featureless Hall state.

Probing the other sectors of the CSL

In the fermionic system, the two topological ground states of the CSL carry momentum $k_y = 0$ and $k_y = \pi$. Due to finite size effects these states are not perfectly degenerate [18, 29]. We prepare these states in our iDMRG simulations by initializing them with product states carrying π momentum in the y-direction. We show the entanglement spectra of the resulting ground states in Fig. S5. As for the trivial sector, we observe a clear separation between bulk

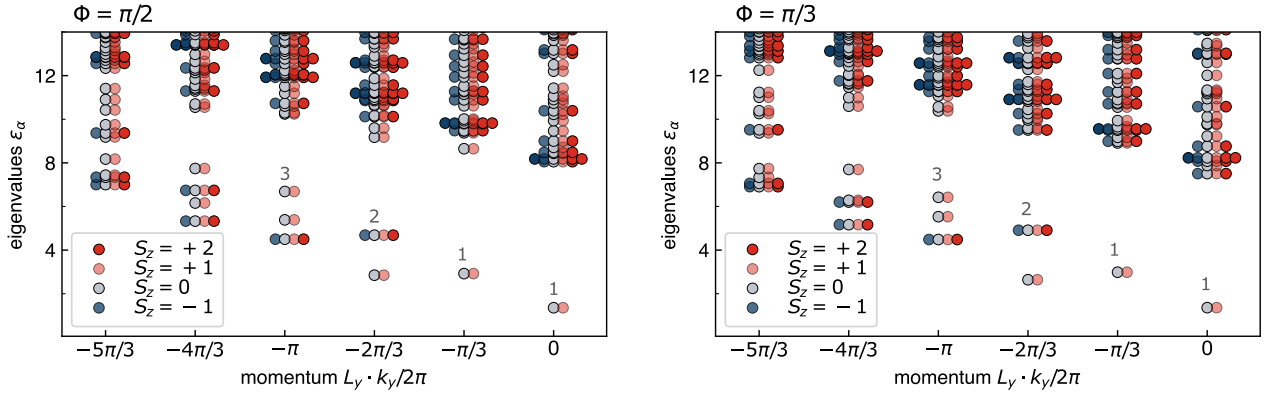


FIG. S5. **Entanglement spectra in the semion sector.** Entanglement spectra in the CSL phase for $U = 15t$ and $\chi = 10000$. For both $\Phi = \pi/2$ (left panel) and $\Phi = \pi/3$ (right panel) the entanglement spectra obey the (1,1,2,3,5,...) counting rule for the edge theory of the CSL. In contrast to the trivial sector, the lowest lying state is now part of a spin 1/2 representation.

and edge modes and the number of dominant eigenvalues in each spin sector continues to follow the (1,1,2,3,...) counting rule. The lowest lying states of the $SU(2)_1$ algebra are now doubly degenerate and are part of a spin 1/2 representation rather than a singlet, see Fig. S5. We remark that instead of preparing finite momentum states via the initial conditions, the two sectors can also be interchanged by threading magnetic flux through the cylinder.